Atmos. Chem. Phys. Discuss., 12, 19617–19647, 2012
www.atmos-chem-phys-discuss.net/12/19617/2012/
doi:10.5194/acpd-12-19617-2012

Atmospheric Chemistry and Physics Discussions

Quantifying the deep convective temperature signal within the tropical tropopause layer (TTL)

L. C. Paulik and T. Birner

Department of Atmospheric Science, Colorado State University, Fort Collins, CO, USA

Received: 21 June 2012 – Accepted: 27 July 2012 – Published: 7 August 2012

Correspondence to: T. Birner (thomas@atmos.colostate.edu)

Published by Copernicus Publications on behalf of the European Geosciences Union.

Abstract

Dynamics on a vast range of spatial and temporal scales, from individual convective plumes to planetary-scale circulations, play a role in driving the temperature variability in the tropical tropopause layer (TTL). Here, we aim to better quantify the deep convective temperature signal within the TTL using multiple datasets. First, we investigate the link between ozone and temperature in the TTL using the Southern Hemisphere Additional Ozonesondes (SHADOZ) dataset. Low ozone concentrations in the TTL are indicative of deep convective transport from the boundary layer. We confirm the usefulness of ozone as an indicator of deep convection by identifying a typical temperature signal associated with reduced ozone events: mid and upper tropospheric warming and TTL cooling. We quantify these temperature signals using two diagnostics: (1) the "ozone minimum" diagnostic, which has been used in previous studies and identifies the upper tropospheric minimum ozone concentration as a proxy for the level of main convective outflow; and (2) the "ozone mixing height", which we introduce in order to identify the maximum altitude in a vertical ozone profile up to which reduced ozone concentrations, typical of transport from the boundary layer are observed. Results indicate that the ozone mixing height diagnostic better separates profiles with convective influence than the ozone minimum diagnostic. Next, we collocate deep convective clouds identified by CloudSat 2B-CLDCLASS with COSMIC GPS temperature profiles. We find a robust large-scale deep convective TTL temperature signal, that is persistent in time. However, it is only the convective events that penetrate into the upper half of the TTL that have a significant impact on TTL temperature. A distinct seasonal difference in the spatial scale and the persistence of the temperature signal is identified. Deep-convective cloud top heights are found to be well described by the level of neutral buoyancy.

ACPD

12, 19617–19647, 2012

1 Background

The interface between the troposphere and the stratosphere is best described as a transition layer. In the tropics, this region is known as the tropical tropopause layer (TTL). The TTL extends from the level of main convective outflow ∼200 hPa to the lower stratosphere ∼70 hPa, and is unique in that it shares both tropospheric and stratospheric characteristics. For example, ozone increases rapidly with height above the level of main convective outflow, whereas temperature continues to decrease up to the cold point tropopause (CPT) ∼100 hPa (Fueglistaler et al., 2009, and references therein). Importance is placed upon this region because it sets the boundary condition for atmospheric tracers entering the stratosphere. Specifically, TTL temperatures control stratospheric water vapor concentrations, which dictate the radiative budget of the stratosphere. Brewer (1949) proposed the "freeze-drying" mechanism in order to explain the very low water vapor concentrations measured throughout the stratosphere: tropospheric air ascending into the stratosphere through the cold tropical tropopause dehydrates to the saturation mixing ratio corresponding to the coldest point along the trajectory. The notion of the Lagrangian cold point determining stratospheric water vapor, which takes into account both horizontal and vertical transport through the TTL is consistent with this picture (e.g. Holton and Gettelman, 2001; Fueglistaler et al., 2005). Because stratospheric water vapor concentrations are linked to TTL temperature and its variability, e.g. clearly seen in the so-called tape recorder signal (Mote et al., 1996), a deep understanding of TTL temperature is desirable. However, the region is complex given that a vast range of spatial and temporal scales affect TTL temperature, and its location makes it susceptible to both stratospheric and tropospheric influence.

While, from above, the global-scale stratospheric circulation significantly influences the temperature and composition of the TTL, tropical deep convection, from below, has the capacity to transport air from the boundary layer to TTL altitudes on the timescale of 1–2 h and create significant temperature anomalies within the TTL. Previous studies have found ozone to be a useful indicator of deep convection, where low ozone

ACPD
12, 19617–19647, 2012

concentrations in the TTL are indicative of deep convective transport from the boundary layer (Kley et al., 1996; Folkins et al., 1999). In turn, this transport alters the region's radiative budget. Steady convective influence maintains the lapse rate in the upper troposphere near the moist adiabatic lapse rate (Folkins and Martin, 2005); however, increasing stratospheric control causes the lapse rate to decrease. The point where the lapse rate diverges from the moist adiabat defines the lapse rate maximum (LRM)[1]. While deep convection can penetrate past the LRM, this level gives an indication of where convective influence predominantly subsides (Gettelman and Forster, 2002). The LRM tends to occur at a higher altitude in regions with a high frequency of deep convection, resulting in a typical longitudinal structure with higher LRM over the west pacific and Africa (Gettelman and Birner, 2007).

The lapse rate changes arise from temperature anomalies created by deep convection. Randel and Wu (2003) and Gettelman and Birner (2007) successfully revealed the regional convective temperature signal when looking at temperature departures from the January zonal mean. The signal is characterized by tropospheric warming up to 150 hPa and cooling maximizing at the CPT, and corresponds to the generic convective signal as first revealed in radiosonde data by Johnson and Kriete (1982). The warming represents the direct response to the deep convective latent heating, while the cooling represents an indirect response to the warming. Holloway and Neelin (2007) described the cooling, or so-called "convective cold top", as a natural response to the convective heating. Their results from a simple hydrostatic model indicated the cooling is the result of horizontal pressure gradients that extend above the heating leading to divergence aloft. Rising motion occurs in order to conserve mass, and this rising motion causes adiabatic cooling to occur. Norton (2006) described the cold anomaly as a wave response to tropospheric diabatic heating, signifying the presence of a zonal-mean wave-driven circulation generated by equatorial Rossby waves (i.e. different from

[1]Note, the LRM has been used in some past studies to refer to the minimum of the potential temperature gradient. Here, we adopt the more straightforward definition based on the conventionally defined lapse rate as the rate of decrease of temperature with height ($-\frac{\partial T}{\partial z}$).

ACPD
12, 19617–19647, 2012

the stratospheric meridional circulation which is driven by extratropical waves). Furthermore, a cold anomaly near the tropopause is a common feature associated with convectively coupled equatorial waves (e.g. Kiladis et al., 2009), and the Madden-Julian Oscillation (e.g. Ma and Kuang, 2011).

Sherwood and Wahrlich (1999) and Sherwood et al. (2003) studied the convective temperature signal at tropical radiosonde stations associated with low satellite brightness temperatures. More recently, Folkins et al. (2008) successfully revealed local convective temperature signals associated with high rainfall rates from the Tropical Rainfall Measuring Mission (TRMM) at tropical radiosonde stations. These earlier studies were limited by (1) using proxies for deep convective clouds (brightness temperature, rain rate), (2) the limited spatial coverage given by the small number of radiosonde station locations. More direct measurements of deep convective cloud tops as well as temperature measurements spanning the entire tropics are required in order to achieve a more complete sense of the structure, scale, and lifetime of the deep convective temperature signal in the TTL and its associated consequences for dehydration. This study combines the use of recent datasets with unprecedented coverage and resolution for characterization of deep convective impact on TTL temperatures.

This paper will proceed by describing the data and prescribed methods in Sect. 2. Section 3 presents results from the Southern Hemisphere Additional Ozonesondes (SHADOZ) dataset, where ozone is used to identify the convective temperature signal. Section 4 presents results based on satellite data from the CloudSat and Constellation Observing System for Meteorology Ionosphere and Climate (COSMIC) missions that describe the structure, scale, and lifetime of the convective temperature signal. Finally, Sect. 5 combines the use of SHADOZ and CloudSat data in a discussion of convective influence on TTL properties.

ACPD
12, 19617–19647, 2012

2 Data and methods

Quantifying convective influence on the TTL strongly benefits from the use of multiple datasets. Here, we describe the datasets utilized in this study and motivate why observing the TTL in this way is useful. First, we use tropospheric ozone measurements to gain insight into deep convective influence. Low ozone concentrations in the upper troposphere, referred to as reduced ozone events, indicate deep convective transport from the boundary layer (Kley et al., 1996; Folkins et al., 1999, 2002). Figure 1 provides a schematic for understanding ozone as an indicator of deep convection. The marine boundary layer maintains low ozone concentrations ($\sim$ 20 ppbv) due to chemical ozone destruction in the presence of sufficient sunlight, high water vapor, and low nitric oxide (NO) concentrations. While ozone concentrations typically increase from the surface up to the tropopause, low ozone concentrations at the surface may be transported to the upper troposphere within deep convective plumes and detrained at the level of convective outflow. Hence, low ozone concentrations in the upper troposphere can diagnose a recent convective event. Entrainment mixes environmental air into the convective updraft diluting the plume, yet ozone is still an effective tracer for diagnosing deep convection.

Beginning in 1998, the Southern Hemisphere Additional Ozonesondes (SHADOZ) data set provides consistent ozone soundings in regions lacking data (Thompson et al., 2003a,b). Balloon-borne electrochemical concentration cell (ECC) ozonesondes measure ozone via a reaction with potassium iodide (Komhyr et al., 1995). Ozonesondes are flown with standard radiosondes to concurrently obtain vertical profiles of standard meteorological variables (such as temperature and pressure). In this study, we examine data from 1998-2009 at ten SHADOZ stations located throughout the tropics: Ascension Island (7.98° S, 14.42° W); Suva, Fiji (18.13° S, 178.4° E); Hilo, Hawaii (19.4° N, 155.0° W); Watukosek, Java (7.57° S, 112.56° E); Kuala Lumpur, Malaysia (2.73° S, 101.7° E); Nairobi, Kenya (1.27° S, 36.8° E); Natal, Brazil (5.42° S, 35.38° W); Paramaribo, Suriname (5.81° N, 55.21° W); Pago Pago, American Samoa (14.23° S,

ACPD
12, 19617–19647, 2012

170.56° W); San Cristobal (0.92° S, 89.60° W). The American Samoa station is of particular interest for looking at ozone as an indicator of deep convection because it has a pristine marine environment and is located in the west Pacific where there is a high occurrence rate of deep convection (Fig. 2). While reduced ozone events are not a direct observation of a deep convective plume, here they are used as proxy to better understand the convective temperature signal.

CloudSat 2B-CLDCLASS offers direct observation of clouds associated with deep convective events that we use as an alternative tool for quantifying convective influence on the TTL. The CloudSat mission, launched in June 2006, provides vertical distributions of hydrometeors using a 94-GHz Cloud Profiling Radar (Stephens et al., 2002), and the CloudSat data product, 2B-CLDCLASS, identifies eight cloud types by means of radar reflectivity (Sassen and Wang, 2008). With this algorithm, we can determine cloud penetration into the TTL by locating deep convective cloud top pixels. We accomplish this by sorting each 2B-CLDCLASS granule, identifying pixel columns that contain deep convective clouds. If a column is flagged as containing a deep convective cloud, the height, location, and time of the maximum deep convective cloud pixel is recorded. A record of deep convective cloud tops pixels between June 2006–April 2011 is used for this study. Figure 2 shows deep convective cloud top pixels exceeding 15 km (yellow), representing cloud tops in the upper half of the TTL or above, and 17 km (red), representing cloud tops above the approximate height of the CPT during all December-January-February (DJF) seasons. About 17 % of all DJF deep convective cloud top heights within [20° S,0°] are greater than 15 km, whereas only ∼ 1 % are greater than 17 km. For reference, we note the median deep convective cloud top height is 12.93 km in DJF [20° S,0°].

In order to uncover deep convective influence on temperature, an investigation of the temperature anomaly at the time and location of a deep convective event is necessary. This requires a high-resolution temperature data set with good spatial and temporal coverage, which ideally does not rely on model output. Here, deep convective cloud top pixels are collocated with COSMIC global positioning system (GPS) temperature

ACPD
12, 19617–19647, 2012

profiles. Like CloudSat, the COSMIC mission provides recent data with global coverage; together they allow for characterization of the deep convective temperature signal in the TTL based purely on observational data with unprecedented detail and spatial coverage. Within 17 months of its launch in April 2006, the COSMIC mission achieved global coverage with ∼2000 soundings per day (Anthes et al., 2008). COSMIC uses radio occultation described extensively by (Kursinski et al., 1997). This technique exploits the bending angle to calculate the vertical profile of refractivity. The equation below, taken from Anthes et al. (2008), shows that the refractive index depends on temperature (T; K), pressure (p; hPa), partial pressure of water vapor (e; hPa), and electron density (n_e; number of electrons per cubic meter), where f is the frequency of the transmitter (Hz).

$$N = 77.6\frac{p}{T} + 3.73 \times 10^5 \frac{e}{T^2} + 4.03 \times 10^7 \frac{n_e}{f^2} \quad (1)$$

Below 90 km, the refractive index depends only on the dry atmospheric density and water vapor density (the first two terms on the right hand side of the equation). The water vapor contribution to the refractive index only becomes important where temperature is greater than 250 K (Kursinski et al., 1996), i.e. below about 7–8 km in the tropics. The temperature is derived from refractive index through integration of the hydrostatic equation. COSMIC uses data assimilation of COSMIC GPS temperature profiles and ECMWF temperature to determine water vapor mixing ratios in the troposphere, providing a temperature profile without the water vapor contribution to the refractive index in the lower tropical troposphere. Here, we use the assimilated temperature profiles but remark that above ∼7–8 km the temperature is essentially COSMIC GPS temperature. Our record of COSMIC GPS temperature profiles are from April 2006–December 2010, mostly overlapping the time period of CloudSat data, and profiles extend from the surface up to 40 km and have 200 m vertical resolution. They are available for download at http://cosmic-io.cosmic.ucar.edu/cdaac/products.html.

ACPD
12, 19617–19647, 2012

3 Results based on SHADOZ data

Several studies have examined the connection between vertical distribution of tropospheric ozone in the tropics and deep convection. Folkins et al. (1999) found ozone to be useful as an indicator of deep convection by identifying similar variability between upper tropospheric ozone and the lapse rate. The lapse rate transition in the upper troposphere (i.e. LRM) coincides with the exponential increase of ozone into the stratosphere. This indicates that the ozone increase is associated with the reduction of convective transport from the surface. Folkins et al. (2002) used the SHADOZ dataset to further this research, noting the average profile of ozone is "S" shaped, with the minimum ozone concentration located at the surface, a local maximum in the lower troposphere ($\sim$ 6.5 km), a local minimum in the upper troposphere ($\sim$ 12 km), and an exponential increase into the stratosphere. The ozone minimum in the upper troposphere indicates convective influence caused by transport of low ozone values from the boundary layer. However, results also showed that considerable differences exist between SHADOZ stations, with the lowest upper tropospheric ozone minimum concentrations occurring at stations with active marine convection. Solomon et al. (2005) found that the southwest Pacific more frequently observes low ozone concentration in the upper troposphere or so-called reduced ozone events, when compared to other regions. The location of these reduced ozone events corresponds to a region of high sea surface temperatures and enhanced deep convection. While the above studies highlight the suitability of ozone as a tracer of deep convection, the present study further analyzes convective influence on ozone profiles. Our aim is to identify and quantify a convective temperature signal associated with reduced ozone events.

In order to identify this signal, we first investigate the temperature profiles associated with the 10 % lowest ozone anomalies at a given vertical level around the main convective outflow layer. Note that this results in a different group of profiles for each vertical level where the ozone anomalies are taken. The temperature profiles are obtained from the radiosonde measurements accompanying each ozonesonde ascent. All anomalies

ACPD
12, 19617–19647, 2012

are created by deseasonalization, which removes the appropriate long-term daily mean profile. Because the level of convective outflow varies, the temperature signal associated with the (10 % lowest) ozone anomalies is taken at each 50 m interpolated level between 10–22 km. We expect a corresponding temperature anomaly profile that exhibits upper tropospheric warming associated with enhanced latent heating, as well as near tropopause cooling associated with the "convective cold top" (see introduction). Figure 3 shows the temperature anomaly at various heights, contoured as a function of the height at which the low ozone anomaly is taken. Anomalies that exceed a 95 % significance level by the difference of means testing appear in color.

A convective temperature signal is evident for low ozone anomalies between 12–18 km. Cooling at the level of the ozone anomaly in the stratosphere (along the dashed line in Fig. 3) is the result of anomalies in vertical motion: ozone is a quasi-passive tracer at these altitudes; anomalously strong upwelling results in anomalously low ozone via advection from below with concurrent local cooling. The strongest convective signal occurs for low ozone anomalies at ∼ 16 km, i.e. somewhat above the level of main convective outflow (∼ 12–14 km). This suggests that profiles with anomalously low ozone concentrations in the upper troposphere and TTL are in fact convectively influenced; deep convection, which triggers the transport of reduced surface ozone concentrations to the upper troposphere, also affects the temperature of the TTL by warming the upper troposphere and cooling the CPT. Because temperature anomalies appear convectively influenced for a range of ozone anomaly heights (between 12–18 km), reduced ozone events appear to manifest themselves within the entire layer. Having established that there is a convective temperature signal associated with low ozone anomalies at the level of convective outflow, we next look at diagnostics to better quantify deep convective influence on individual profiles.

The "ozone minimum" diagnostic, discussed in previous studies (Gettelman and Forster, 2002; Gettelman and Birner, 2007), provides a way to quantify the nature of the "S" shape in individual profiles by identifying the location and strength of the upper tropospheric ozone minimum. Here, the ozone minimum is defined as the lowest

ACPD
12, 19617–19647, 2012

ozone concentration above 6.5 km in a given profile. The height requirement is in place to ensure the event is upper tropospheric, and 6.5 km is chosen because it is the level in "S" shaped ozone profile where concentrations begin to decrease toward the upper tropospheric minimum. The ozone minimum generally occurs just above the LRM (Gettelman and Forster, 2002).

Figure 4 shows an individual ozone profile at American Samoa chosen because it exemplifies the "S" shape described by Folkins et al. (2002). However, it also demonstrates that ozone may remain low over a layer in the upper troposphere, a typical structure seen in the majority of ozone profiles. Here, we see the ozone minimum occurs at 10.15 km; however, ozone concentrations are similar to the concentration at the minimum between ∼9–14 km, which renders the precise value of the ozone minimum height somewhat irrelevant. Rather than identifying the upper tropospheric ozone minimum, a new diagnostic, "ozone mixing height", is established to determine the maximum height up to which reduced ozone concentrations of a given threshold, typical of transport from the boundary layer, are observed. In defining the threshold concentration, we utilize the level of neutral buoyancy (LNB).

Defined as the level at which a parcel rising adiabatically within a convective updraft will no longer be positively buoyant, the LNB offers a useful way to quantify the potential upper extent of deep convective influence. Once a parcel reaches this level, it will likely detrain and mix with the environment. Because low ozone concentrations at the surface have the potential to be mixed up to LNB via deep convective updrafts, this parameter may be thought of as an upper bound for vertical ozone mixing. Thus, the threshold concentration for the "ozone mixing height" diagnostic is determined by averaging ozone concentrations at the LNB during each season to give a typical concentration of ozone at the detrainment level. The LNB is obtained here assuming pseudo-adiabatic ascent and using an air parcel origin that maximizes convective available potential energy (CAPE). The CAPE calculation is standard in that it neglects entrainment and does not take into account latent heat of fusion. In Fig. 4, the ozone mixing height occurs

ACPD
12, 19617–19647, 2012

at 13.6 km, which is the maximum altitude ozone is less that the 33.4 ppbv threshold concentration.

For both diagnostics, we produce composites with respect to either the height of the ozone minimum or the ozone mixing height, in order to determine the temperature fields associated with differing levels of main convective influence.

Figure 5 (top) displays the composite temperature anomaly profiles sorted by the ozone mixing height, where colored lines indicate that the anomaly meets the 95 % significance level. A strong convective temperature signal characterized by warming in the upper troposphere and a cooling maximizing at the CPT appears for the 10 % highest ozone mixing heights. A similar, though somewhat weaker signal appears for anomalously high, but not extremely high ozone mixing heights (labeled 70–90 % in the plot). These signals represent the large-scale temperature signature of deep convection, and suggest anomalously high ozone mixing heights in fact represent convectively influenced profiles. It is also interesting to note the 10 % lowest ozone mixing heights have a reverse signal (cool upper tropospheric anomaly, warm CPT anomaly), i.e. a clear transition between a convective and non-convective regime is evident. While there is a strong change in the temperature at the approximate level of CPT, the average height of the CPT does not change between composite groups. Compositing lapse rate profiles with respect to the ozone mixing height reveals a shift in the height of the lapse rate decrease associated with the transition into a stratospheric regime; high altitude ozone mixing heights have higher altitude lapse rate decreases (not shown).

Figure 5 (bottom) shows similar composites using the ozone minimum height diagnostic. There is also evidence of a convective temperature signal associated with the 10 % highest ozone minimum heights; however, the magnitude of the signal is strongly reduced when compared to the highest ozone mixing heights. Furthermore, the 10 % lowest ozone minimum heights do not show a clear reverse signal, and a transition from the convective to the non-convective regime is not readily apparent.

Here, we have found temperature to have a deep convective signal associated with the reduced ozone events. Results suggest that using the LNB in connection with

ACPD
12, 19617–19647, 2012

vertical ozone profile is effective for determining convective influence. Results based on the ozone minimum diagnostic do not provide as clear a picture of this convective influence.

4 Results based on CloudSat and COSMIC data

Having identified a deep convective temperature signal associated with reduced ozone events, we now investigate the signal associated with direct observations of deep convective clouds. Our approach collocates deep convective cloud top pixels identified by CloudSat 2B-CLDCLASS with COSMIC GPS temperature profiles. COSMIC GPS temperature profiles are deseasonalized by creating monthly mean profiles at each point on a $5^\circ \times 5^\circ$ grid and removing the long-term monthly mean profile interpolated to each profile location. Given that the GPS signal enters the atmosphere at an angle, the interpolation accounts for variations in profile location at each vertical level. The presented results collocate deep convective clouds to the location of the sounding at 17 km, the approximate height of the CPT; however, results are similar when collocating to the location of the sounding in the upper troposphere where deep convective heating is expected. The method ignores the time it takes for a GPS temperature profile to pass through the atmosphere (this is of the order of a few minutes, which is much shorter than the shortest possible distance in time used for the collocation). The distance between deep convective clouds and temperature profiles is computed using the Great Circles Distance Formula:

$$\text{Distance} = a \times \arccos[\sin\varphi_1 \sin\varphi_2 + \cos\varphi_1 \cos\varphi_2 \cos(\lambda_2 - \lambda_1)]. \quad (2)$$

In this formula, a is the radius of the earth (6378.7 km), λ is longitude, and φ is latitude, with indices 1 and 2 referring to the locations of the cloud and temperature observations, respectively. Variations in a are ignored because only the tropics are considered.

ACPD
12, 19617–19647, 2012

Using this method, we are able to quantify the temperature signal of deep convection, characterized by deep upper tropospheric warming and CPT cooling, for temperature profiles in proximity to deep convective cloud top pixels. Results indicate the temperature signal is strongly dependent on the height of the deep convective cloud top pixel. Figure 6 shows the (top) DJF and (bottom) June-July-August (JJA) average profiles of the temperature anomaly within 1000 km associated with various deep convective cloud top pixel heights, where colored lines indicate anomalies that exceed a 99 % significance level. We have restricted the latitude in each season in order to account for the seasonal shift in deep convection; for DJF we use deep convective cloud top pixels between [20° S,0°], while for JJA we use deep convective cloud top pixels between [0°,20° N]. It is clear that the strongest convective temperature signal appears for temperature profiles in proximity to the highest deep convective clouds in both seasons. The temperature signal for deep convective cloud tops greater than 17 km in DJF shows warming between 3–15 km, with the strongest warming (∼ 1 K) occurring at ∼ 12 km, and cooling between 15–18 km, with the strongest cooling (∼ −1.5 K) occurring at ∼ 17 km. The magnitude of the maximum cooling and heating is smaller, and occurs at lower altitudes for deep convective cloud tops between 16–17 km (maximum cooling of 0.5 K occurs at ∼ 16 km). Cooling and warming shifts down and the magnitude is further reduced for deep convective cloud tops between 15–16 km, and the convective temperature signal disappears for deep convective cloud tops lower than 15 km. This suggests that only the deep convective clouds that penetrate into the upper half of the TTL or above (> 15 km) affect TTL temperature. And, while deep convective cloud top pixels greater than 17 km are rare and only occur in localized regions (Fig. 2), they appear to have the greatest impact. The remainder of this section investigates the temperature signal in proximity to deep convective cloud top pixels greater than 17 km.

First, the dependence of the signal on the distance between the deep convective cloud top pixel and the COSMIC GPS temperature profile is investigated. Figure 7 shows the temperature anomaly contoured as a function of the distance between the deep convective cloud top pixel and the COSMIC GPS temperature profile and altitude.

ACPD
12, 19617–19647, 2012

Anomalies appear in color when they exceed the 99 % significance level. As expected, the magnitude of the anomalies decays with increasing distance. It is also apparent that the anomalies decay faster with increasing distance in JJA, becoming insignificant beyond ∼ 1500 km. The anomalies in DJF are more persistent, having an impact out to ∼ 3500 km away from the convective event. We conclude that the signal is large-scale, having an impact on TTL temperatures as far as several thousand kilometers away from the deep convective event, but there is evidence that a distinct difference in the spatial scale exists between seasons.

Using our collocation method, we can also investigate the time evolution of a convective event to provide insight into the system's lifecycle. Figure 8 shows the average temperature anomaly within 1000 km of a deep convective cloud top pixel greater than 17 km contoured as a function of lag, where colored anomalies exceed the 99 % significance level. During DJF, the convective temperature anomaly starts to exceed 0.5 K in the upper troposphere ∼ 4 days preceding the deep convective event. Evidence of a strong signal earlier than the observed deep convective cloud (less than day 0) suggests convective influence began before CloudSat observed the deep convective cloud top. A strong signal up to a week after the convective event (∼ 8 days in DJF) indicates its persistence in time. The temperature anomaly in JJA is significantly shorter-lived demonstrating a noteworthy difference between seasons, similar to the difference in spatial scales. We note that the negative anomaly at the CPT appears to somewhat precede the strongest upper tropospheric warming, perhaps indicating destabilization of the upper troposphere prior to a convective event.

This section successfully revealed the convective temperature signal associated with observed deep convective clouds. Results suggest only convection that penetrates into the upper half of the TTL (> 15 km) has a significant impact on the temperature distribution of the TTL. Now, using results from Sect. 3, we look to draw conclusions about deep convection in the upper half of the TTL.

ACPD
12, 19617–19647, 2012

5 Discussion

We have used two approaches to better understand the temperature signal associated with deep convection. The first approach utilized the SHADOZ dataset, investigating ozone as a tracer for deep convection. A convective signal in temperature was identified for the 10 % lowest ozone anomalies between 12–18 km (Fig. 3), confirming ozone as an effective tracer for deep convection. The strongest signal was observed for low ozone anomalies above 15 km, corresponding to the upper half of the TTL. We quantified convective influence from individual ozone profiles based on two diagnostics: the height of the lowest ozone mixing ratio (the "ozone minimum") and the height up to which ozone stays below a certain threshold concentration (the "ozone mixing height"). The level of neutral buoyancy (LNB) was utilized to define the threshold for the ozone mixing height. Compositing with respect to the ozone mixing height, as opposed to the ozone minimum height, better separated profiles with convective influence; the 10 % highest ozone mixing heights reflect profiles with a strong convective temperature signal. Thus, we conclude that ozone mixing height is a more effective diagnostic for assessing convective influence.

The second approach used CloudSat 2B-CLDCLASS data. Identified deep convective cloud top pixels were collocated with COSMIC GPS temperature profiles. The strongest convective temperature signal appeared for deep convective cloud top pixels within the upper half of the TTL or above (> 15 km), consistent with our results based on ozone (see above). Results show that the convective temperature signal is large-scale and persistent in time, with a distinct difference between the seasons: during DJF the signal tends to be larger in scale and more persistent in time than during JJA. In summary, individual approaches based on SHADOZ and CloudSat/COSMIC GPS revealed distinct deep convective temperature signals in the TTL. We will now combine both approaches in order to provide a more synergistic understanding of deep convective influence on temperature in the TTL.

ACPD
12, 19617–19647, 2012

The locations of the SHADOZ stations relative to the occurrence of deep convective cloud top pixels as identified by CloudSat are shown in Fig. 2. To better understand convection at each SHADOZ station, we produce a climatology of deep convective cloud top heights by identifying cloud top pixels within 1000 km of a given station. Figure 9 (top) presents this climatology for the American Samoa station, where the relative frequency of identified deep convective cloud top pixels is contoured as a function of month and height. Here it is seen that deep convection most frequently occurs in December–April. These months display a bimodal distribution in deep convective cloud top pixel height with a dominant peak near 15 km and a secondary peak between 7–8 km. This secondary peak seems to indicate the presences of high cumulus congestus cloud tops, falsely categorized as deep convective cloud tops. Plotted over the deep convective cloud climatology is the annual cycle of the LNB (only using those located above 6.5 km) and the ozone mixing height. The LNB and the ozone mixing height tend to occur at roughly the same altitude as the deep convective cloud tops. In contrast, the LRM and the ozone minimum height do not appear to represent deep convective cloud tops as well.

Figure 9 (bottom) shows the annual cycle of ozone mixing ratio contoured as a function of height at American Samoa, similar to Fig. 3d in Thompson et al. (2011). Here, it is seen that upper tropospheric ozone concentrations are lower in months with a high frequency of deep convection, most notably the 30 ppbv contour occurs at ∼ 14 km during the convective season and ∼ 4 km during the non-convective season. A strong transition between the tropospheric and stratospheric chemical regime occurs at ∼ 15 km with a stronger gradient during the convective season. Because the LNB and convective cloud tops also subside at ∼ 15 km, deep convection is concluded to be significant in influencing composition up to this level during the convective season. While Folkins et al. (2002) showed convective detrainment to decrease above ∼ 12.5 km, our results suggest a slightly higher detrainment altitudes and a well-mixed troposphere up to the LNB.

ACPD
12, 19617–19647, 2012

Combining SHADOZ and CloudSat has shown that the height of deep convective cloud tops is well represented by the LNB. The calculation of the LNB assumes (1) undiluted ascent (which Romps and Kuang, 2010, find to be extremely unlikely for plumes reaching TTL altitudes), and does not account for the effects of (2) latent heat due to freezing (which provides additional parcel buoyancy, e.g. Fierro et al., 2009), and (3) overshoots. Assumption (1) results in an overestimation, while both (2) and (3) result in an underestimation of the height of the LNB. The strong agreement between deep convective cloud top heights and the LNB therefore suggests that these competing neglected effects roughly cancel – the (conventional) LNB appears to effectively define the maximum vertical extent of deep convective influence. The lapse rate maximum (LRM) height, in contrast, does not appear to provide a similarly effective diagnostic. Because the convective temperature signal appeared strongest for ozone anomalies in the upper half of the TTL (> 15 km) and for convective cloud top pixels that penetrate to the upper half of the TTL, we conclude that it is only the highest deep convective events that have a significant impact on TTL temperature and composition.

Utilizing recently developed datasets (in particular based on the Cloud Profiling Radar on CloudSat and the GPS radio occultations from COSMIC) allowed us to provide an improved quantification of the structure, scale, and persistence of convectively induced temperature variability in the TTL. The conveyed information may prove useful for the development and representation of crucial TTL properties in climate models.

Acknowledgements. This work originated out of LCP's M.Sc. thesis at Colorado State University – discussions and suggestions by her committee members (Colette Heald, Graeme Stephens, David Krueger) are gratefully acknowledged. LCP was funded through NASA grant #NAS5-99237 (CloudSat). TB acknowledges current funding through a CAREER grant by the US National Science Foundation (NSF).

ACPD
12, 19617–19647, 2012

References

Anthes, R. A., Kallberg, P. W., Simmons, A. J., Andrae, U., Bechtold, P., Costa, V. D., M. Fiorino, M., Gibson, J. K., Haseler, J., Hernandez, A., Kelly, G. A., Li, X., Onogi, K., Saarinen, S., Sokka, N., Allan, R. P., Andersson, E., Arpe, K., Balmaseda, M. A., Beljaars, A. C. M., Berg, L. V. D., Bidlot, J., Bormann, N., Caires, S., Chevallier, F., Dethof, A., Dragosavac, M., Fisher, M., Fuentes, M., Hagemann, S., Holm, E., Hoskins, B. J., Isaksen, L., Janssen, P. A. E. M., Jenne, R., McNally, A. P., Mahfouf, J.-F., Morcrette, J.-J., Rayner, N. A., Saunders, R. W., Simon, P., Sterl, A., Trenberth, K. E., Untch, A., Vasiljevic, D., Viterbo, P., and Woollen, J.: The COSMIC/FORMOSAT-3 mission: Early results, B. Am. Meteor. Soc., 89, 313–333, 2008. 19624

Brewer, A. W.: Evidence for a world circulation provided by the measurements of helium and water vapor distribution in the stratosphere, Q. J. Roy. Meteorol. Soc., 75, 351–363, 1949. 19619

Fierro, A. O., Simpson, J., LeMone, M. A., Straka, J. M., and Smull, B. F.: On how hot towers fuel the Hadley cell: An observational and modeling study of line-organized convection in the equatorial trough from TOGA COARE, J. Atmos. Sci., 66, 2730–2746, 2009. 19634

Folkins, I. and Martin, R. V.: The vertical structure of tropical convection and its impact on the budgets of water vapor and ozone, J. Atmos. Sci., 62, 1560–1573, 2005. 19620

Folkins, I., Loewenstein, M., Podolske, J., Oltmans, S. J., and Proffitt, M.: A barrier to vertical mixing at 14 km in the tropics: Evidence from ozonesondes and aircraft measurements, J. Geophys. Res., 104, 22095–22102, 1999. 19620, 19622, 19625

Folkins, I., Braun, C., Thompson, A. M., and White, J.: Tropical ozone as indicator of deep convection, J. Geophys. Res., 107, 4184, doi:10.1029/2001JD001178, 2002. 19622, 19625, 19627, 19633

Folkins, I., Fueglistaler, S., Lesins, G., and Mitovski, T.: A Low-Level Circulation in the Tropics, J. Atmos. Sci., 65, 1019–1034, 2008. 19621

Fueglistaler, S., Bonazzola, M., Haynes, P. H., and Peter, T.: Stratospheric water vapor predicted from Lagrangian temperature history of air entering the stratosphere in the tropics, J. Geophys. Res., 110, D08107, doi:10.1029/2004JD005516, 2005. 19619

Fueglistaler, S., Dessler, A. E., Dunkerton, T. J., Folkins, I., Fu, Q., and Mote, P. W.: Tropical tropopause layer, Rev. Geophys., 47, RG1004, doi:10.1029/2008RG000267, 2009. 19619

ACPD
12, 19617–19647, 2012

Gettelman, A. and Birner, T.: Insights into Tropical Tropopause Layer processes using global models, J. Geophys. Res., 112, D23104, doi:10.1029/2007JD008945, 2007. 19620, 19626
Gettelman, A. and Forster, P. M. d. F.: A climatology of the tropical tropopause layer, J. Meteor. Soc. Japan, 80, 911–924, 2002. 19620, 19626, 19627
Holloway, C. E. and Neelin, J. D.: The convective cold top and quasi equilibrium, J. Atmos. Sci., 64, 1467–1487, 2007. 19620
Holton, J. R. and Gettelman, A.: Horizontal transport and the dehydration of the stratosphere, Geophys. Res. Lett., 28, 2799–2802, 2001. 19619
Johnson, R. H. and Kriete, D. C.: Thermodynamic and circulation characteristics of winter monsoon tropical mesoscale convection, Mon. Weather Rev., 110, 1898–1911, 1982. 19620
Kiladis, G. N., Wheeler, M. C., Haertel, P. T., Straub, K. H., and Roundy, P. E.: Convectively coupled equatorial waves, Rev. Geophys., 47, RG2003, doi:10.1029/2008RG000266, 2009. 19621
Kley, D., Crutzen, P. J., Smit, H. G. J., Vömel, H., Oltmans, S. J., Grassl, H., and Ramanathan, V.: Observations of Near-Zero Ozone Concentrations over the Convective Pacific: Effects on Air Chemistry, Science, 274, 230–233, 1996. 19620, 19622
Komhyr, W. D., Barnes, R., Brothers, G., Lathrop, J., and Opperman, D.: Electrochemical concentration cell ozonesonde performance evaluation during STOIC 1989, J. Geophys. Res., 100, 9231–9244, 1995. 19622
Kursinski, E. R., Hajj, G. A., Bertiger, W. I., Leroy, S. S., Meehan, T. K., Romans, L. J., Schofield, J. T., McCleese, D. J., Melbourne, W. G., Thornton, C. L., Yunck, T. P., Eyre, J. R., and Nagatani, R. N.: Initial results of radio occultation observations of the Earth's atmosphere using the Global Positioning System, Science, 271, 1107–1110, 1996. 19624
Kursinski, E. R., Haij, G. A., Schofield, J. T., Linfield, R. P., and Hardy, K. R.: Observing the Earth's atmosphere with radio occultation measurements using the Global Positioning System, J. Geophys. Res., 102, 23429–23465, 1997. 19624
Ma, D. and Kuang, Z.: Modulation of radiative heating by the Madden Julian Oscillation and convectively coupled Kelvin waves as observed by CloudSat, Geophys. Res. Lett., 38, L21813, doi:10.1029/2011GL049734, 2011. 19621
Mote, P. W., Rosenlof, K. H., McIntyre, M. E., Carr, E. S., Gille, J. G., Holton, J. R., Kinnersley, J. S., Pumphrey, H. C., Russell, J. M., I., and Waters, J. W.: An atmospheric tape recorder: The imprint of tropical tropopause temperatures on stratospheric water vapor, J. Geophys. Res., 101, 3989–4006, 1996. 19619

ACPD
12, 19617–19647, 2012

Norton, W. A.: Tropical Wave Driving of the Annual Cycle in Tropical Tropopause Temperatures. Part II: Model Results, J. Atmos. Sci., 63, 1420–1431, 2006. 19620

Randel, W. J. and Wu, F.: Thermal variability of the tropical tropopause region derived from GPS/MET observations, J. Geophys. Res., 108, 4024, doi:10.1029/2002JD002595, 2003. 19620

Romps, D. M. and Kuang, Z.: Do Undiluted Convective Plumes Exist in the Upper Tropical Troposphere?, J. Atmos. Sci., 67, 468–484, 2010. 19634

Sassen, K. and Wang, Z.: Classifying clouds around the globe with CloudSat radar: 1-year of results, Geophys. Res. Lett., 35, L04805, doi:10.1029/2007GL032591, 2008. 19623

Sherwood, S. C. and Wahrlich, R.: Observed Evolution of Tropical Deep Convective Events and Their Environment, Mon. Weather Rev., 127, 1777–1795, 1999. 19621

Sherwood, S. C., Horinouchi, T., and Zeleznik, H.: Convective impact on temperatures observed near the tropical tropopause, J. Atmos. Sci., 60, 1847–1856, 2003. 19621

Solomon, S., Portmann, R. W., Sasaki, T., Hofmann, D. J., and Thompson, D. W. J.: Four decades of ozonesonde measurements over Antarctica, J. Geophys. Res., 110, D21311, doi:10.1029/2005JD005917, 2005. 19625

Stephens, G. L., Vane, D. G., Boain, R. J., Mace, G. G., Sassen, K., Wang, Z., Illingworth, A. J., O'Connor, E. J., Rossow, W. B., Durden, S. L., Miller, S. D., Austin, R. T., Benedetti, A., Mitrescu, C., and The CloudSat Science Team: The CloudSat Mission and the A-Train, B. Am. Meteor. Soc., 83, 1771–1790, 2002. 19623

Thompson, A. M., Witte, J. C., McPeters, R. D., Oltmans, S. J., Schmidlin, F. J., Logan, J. A., Fujiwara, M., Kirchhoff, V. W. J. H., Posny, F., Coetzee, G. J. R., Hoegger, B., Kawakami, S., Ogawa, T., Johnson, B. J., Vomel, H., and Labow, G.: Southern Hemisphere Additional Ozonesondes (SHADOZ) 1998–2000 tropical ozone climatology 1. Comparison with Total Ozone Mapping Spectrometer (TOMS) and ground-based measurements, J. Geophys. Res., 108, 8238, doi:10.1029/2001JD000967, 2003a. 19622

Thompson, A. M., Witte, J. C., Oltmans, S. J., Schmidlin, F. J., Logan, J. A., Fujiwara, M., Kirchhoff, V. W. J. H., Posny, F., Coetzee, G. J. R., Hoegger, B., Kawakami, S., Ogawa, T., Fortuin, J. P. F., and Kelder, H. M.: Southern Hemisphere Additional Ozonesondes (SHADOZ) 1998–2000 tropical ozone climatology 2. Tropospheric variability and the zonal wave-one, J. Geophys. Res., 108, 8241, doi:10.1029/2002JD002241, 2003b. 19622

Thompson, A. M., Allen, A. L., Lee, S., Miller, S. K., and Witte, J. C.: Gravity and Rossby wave signatures in the tropical troposphere and lower stratosphere based on South-

ACPD
12, 19617–19647, 2012

ern Hemisphere Additional Ozonesondes (SHADOZ), J. Geophys. Res., 116, D05302, doi:10.1029/2009JD013429, 2011. 19633, 19647

ACPD
12, 19617–19647, 2012

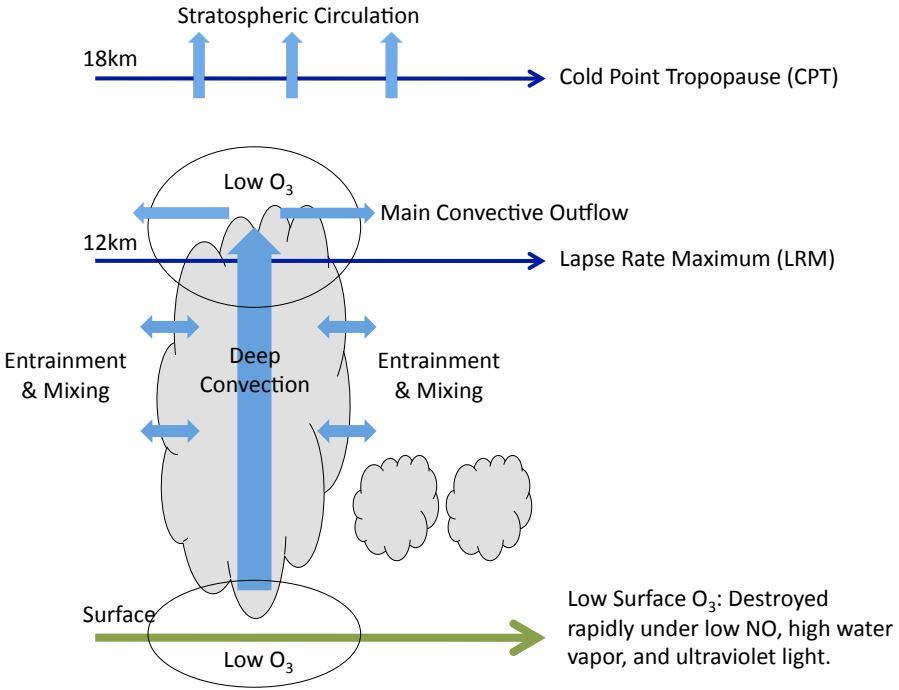

Fig. 1. A conceptual model for understanding ozone as a tracer of deep convection. Low ozone concentrations near the surface can be transported to the upper troposphere within deep convective updrafts and detrained around the level of deep convective outflow. Entrainment and mixing can dilute the updraft, distorting the convective ozone signal.

ACPD
12, 19617–19647, 2012

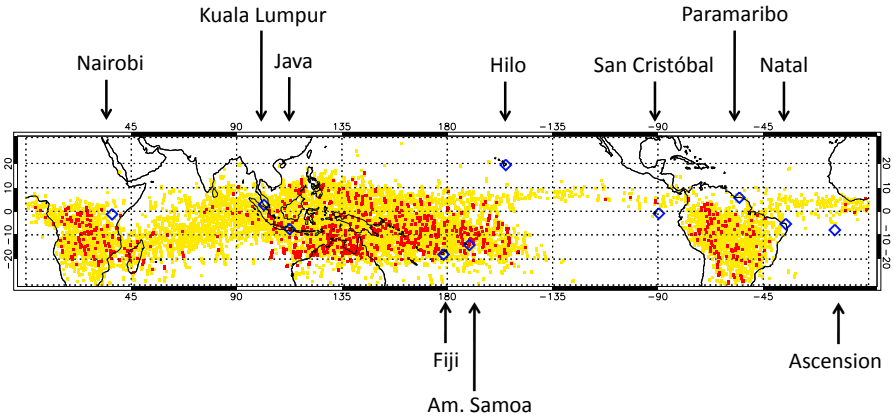

Fig. 2. Spatial distribution of deep convective cloud top pixels greater than 15 km (yellow) and greater than 17 km (red) during DJF. The locations of SHADOZ stations investigated in this study are marked with blue diamonds.

ACPD
12, 19617–19647, 2012

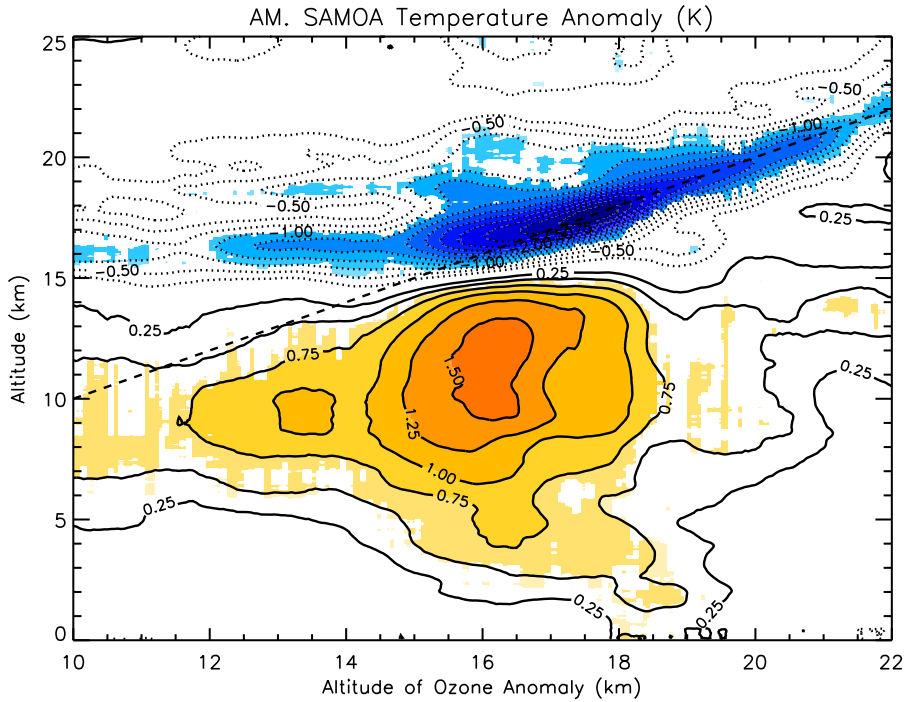

Fig. 3. The average temperature anomaly contoured as a function of altitude (ordinate), corresponding to the 10 % lowest ozone anomalies taken at various altitudes (abscissa), at American Samoa. The contour interval is 0.25 K, with dotted contours indicating negative anomalies. Anomalies that exceed the 95 % significance level appear in color. The 1 : 1 line appears dashed.

ACPD
12, 19617–19647, 2012

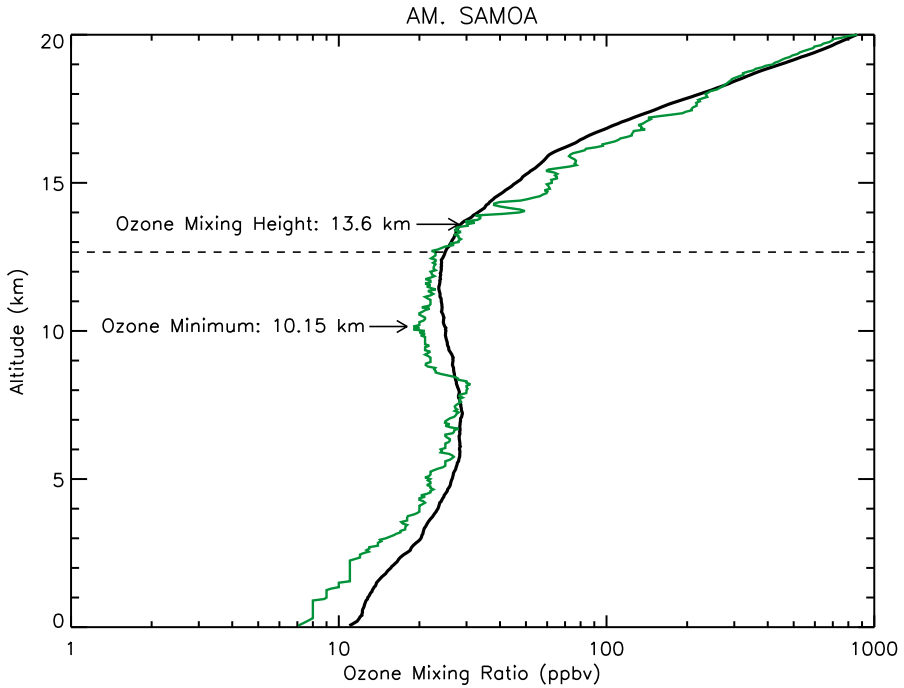

Fig. 4. The vertical ozone profile (green line) from 8 March 2006 at American Samoa demonstrating that ozone can remain relatively low over a layer of substantial thickness in the upper troposphere. The ozone minimum occurs at 10.15 km and the ozone mixing height at 13.6 km (corresponding to the maximum altitude ozone is less than 33.4 ppbv – the seasonally average ozone concentration at the LNB). The seasonal mean (March-April-May) ozone profile is plotted with a black line. The horizontal dashed line indicates the seasonal mean height of the LNB.

ACPD
12, 19617–19647, 2012

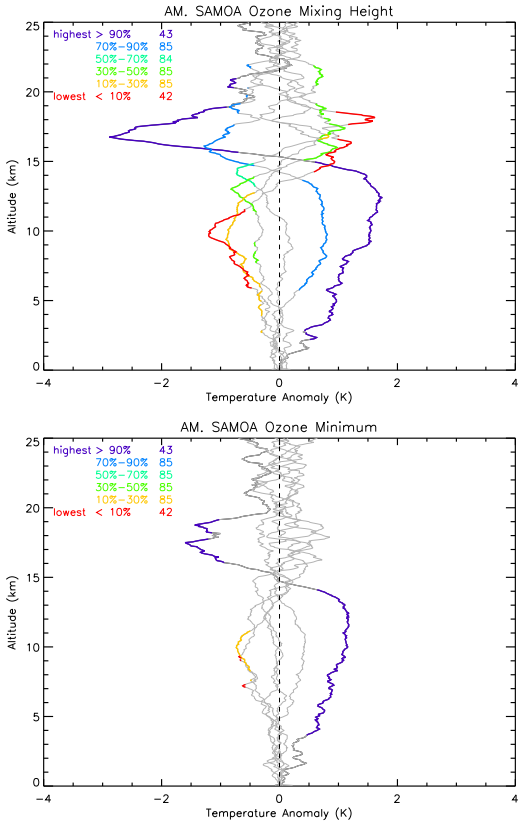

Fig. 5. Average profiles of temperature anomaly composited by (top) the height of the ozone mixing height and (bottom) the ozone minimum. Colored lines indicate where anomalies exceed the 95 % significance level (with blue – highest and red – lowest heights). The number of profiles that make up each composite group appears next to the percentage.

ACPD
12, 19617–19647, 2012

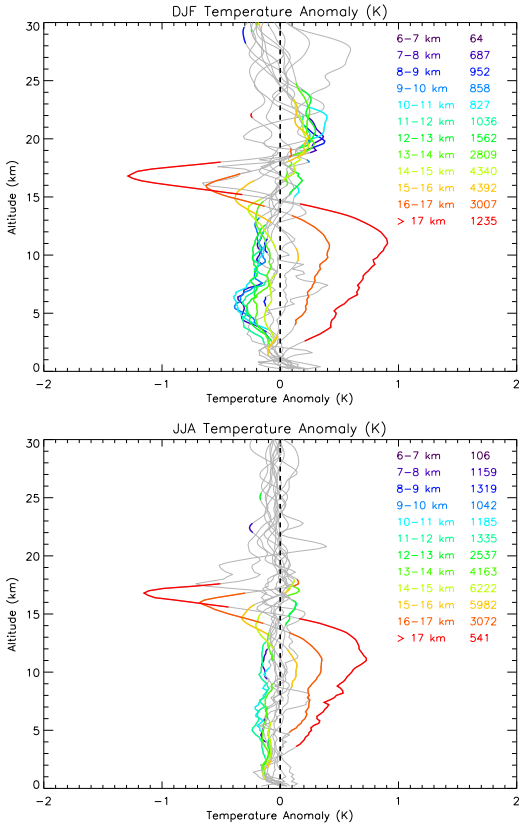

Fig. 6. Average temperature anomaly profiles for GPS soundings within ±6 h and 1000 km of a maximum deep convective cloud greater than 17 km (red), between 16–17 km (orange), between 15–16 km (yellow), etc. during (top) DJF and (bottom) JJA. Anomalies that exceed the 99 % significance level appear in color. The number of profiles that go into each anomaly profile is given on the right side of the figure.

ACPD
12, 19617–19647, 2012

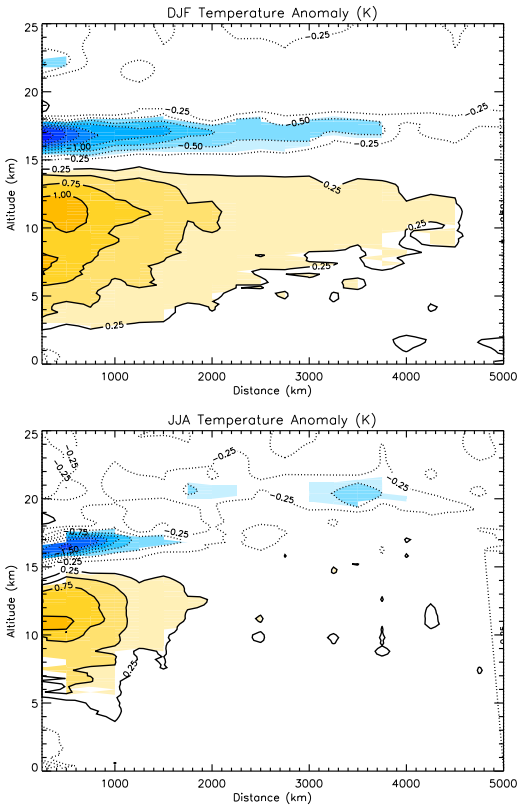

Fig. 7. Temperature anomaly contoured as a function of distance between CloudSat and COSMIC GPS measurements (within ±6 h) and altitude, corresponding to events with deep convective cloud top pixels above 17 km, for (top) DJF and (bottom) JJA. Anomalies that exceed the 99 % significance level appear in color. Orange and red colors correspond to positive anomalies, blue colors correspond to negative anomalies.

ACPD
12, 19617–19647, 2012

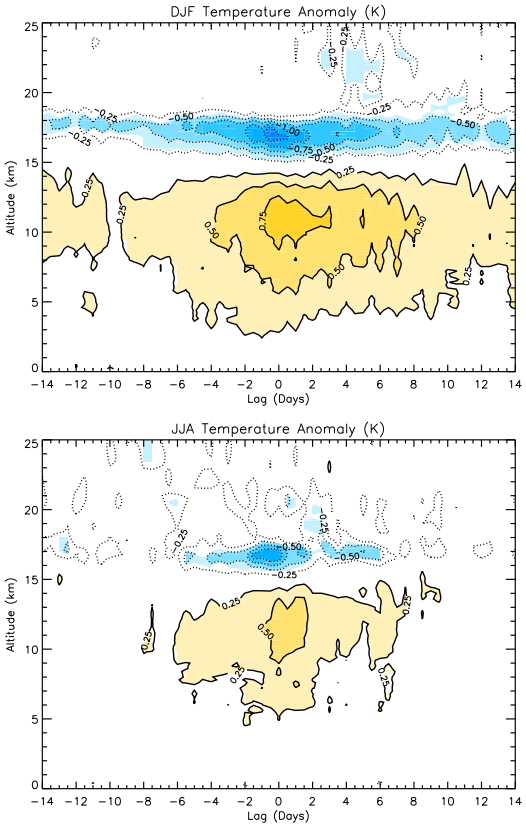

Fig. 8. Temperature anomaly within 0–1000 km of a deep convective cloud top pixel greater than 17 km, contoured as a function of time and altitude during (top) DJF and (bottom) JJA. The contour interval is 0.25 K, and anomalies that exceed the 99 % significance level appear in color. Orange and red colors correspond to positive anomalies, blue colors correspond to negative anomalies.

ACPD
12, 19617–19647, 2012

TTL deep convective temperature signal

L. C. Paulik and T. Birner

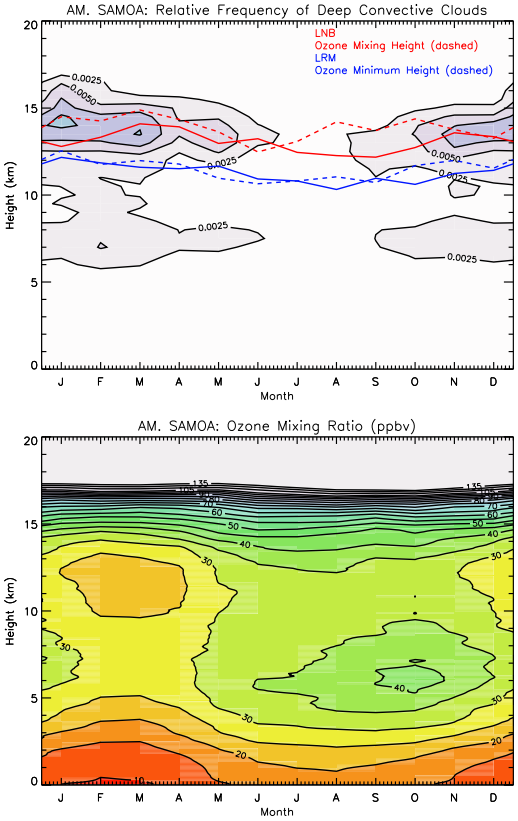

Fig. 9. (top) Annual cycle of deep convective cloud top pixel height within 1000 km of American Samoa. Also included is the annual cycle of the LNB (red, solid), the ozone mixing height (red, dashed), the LRM height (blue, solid), and the ozone minimum height (blue, dashed). (bottom) annual cycle of the ozone concentration (ppbv) at American Samoa, similar to Fig. 3d in Thompson et al. (2011). Orange and red colors indicate relatively low values, blue colors indicate relatively high values.

ACPD
12, 19617–19647, 2012